Fully Coupled Modeling of Burnup-Dependent $(U_{1-y}, Pu_y)O_{2-x}$ Mixed Oxide Fast Reactor Fuel Performance

RONG LIU, WENZHONG ZHOU, and WEI ZHOU

During the fast reactor nuclear fuel fission reaction, fission gases accumulate and form pores with the increase of fuel burnup, which decreases the fuel thermal conductivity, leading to overheating of the fuel element. The diffusion of plutonium and oxygen with high temperature gradient is also one of the important fuel performance concerns as it will affect the fuel material properties, power distribution, and overall performance of the fuel pin. In order to investigate these important issues, the $(U_{1-y}Pu_y)O_{2-x}$ fuel pellet is studied by fully coupling thermal transport, deformation, oxygen diffusion, fission gas release and swelling, and plutonium redistribution to evaluate the effects on each other with burnup-dependent models, accounting for the evolution of fuel porosity. The approach was developed using self-defined multiphysics models based on the framework of COMSOL Multiphysics to manage the nonlinearities associated with fast reactor mixed oxide fuel performance analysis. The modeling results showed a consistent fuel performance comparable with the previous results. Burnup degrades the fuel thermal conductivity, resulting in a significant fuel temperature increase. The fission gas release increased rapidly first and then steadily with the burnup increase. The fuel porosity increased dramatically at the beginning of the burnup and then kept constant as the fission gas released to the fuel free volume, causing the fuel temperature to increase. Another important finding is that the deviation from stoichiometry of oxygen affects greatly not only the fuel properties, for example, thermal conductivity, but also the fuel performance, for example, temperature distribution, porosity evolution, grain size growth, fission gas release, deformation, and plutonium redistribution. Special attention needs to be paid to the deviation from stoichiometry of oxygen in fuel fabrication. Plutonium content will also affect the fuel material properties and performance. However, it is not that significant compared to the deviation from stoichiometry of oxygen due to the similar material properties of UO_2 and PuO_2.

I. INTRODUCTION

MIXED oxide $(U_{1-y}, Pu_y)O_{2-x}$ fuel is widely used in fast reactors and of interest for the Generation-IV nuclear reactors, which is a promising fuel candidate not only to transmute long-life minor actinides in fast breeder reactors (FBRs), but also to establish an FBR cycle with high potential of non-proliferation.[1] Sodium-cooled fast reactors operate with a higher linear heat rate and higher coolant temperature than Lighter Water Reactors (LWRs), and also have a lower fuel smear density and lower initial oxygen-to-metal ratio, resulting in high temperatures, high temperature gradients, and a complex chemical environment, which will cause the migration of fuel constituents and fuel deformation.[2] In addition to chemistry, high temperatures also affect fission gas release and swelling. Surface diffusion may allow bulk intra-granular bubble movement and direct discharge into the grain boundaries. There are some previous works concerning the fuel constituents such as Zr in metallic fuel[3], and oxygen and plutonium redistribution in mixed oxide fuel.[4–6]

Mihaila et al. studied the MOX and UO_2 fuel by coupling heat transport, oxygen diffusion, and thermal deformation with different thermal conductivity models under a variety of initial and boundary conditions, indicating sensitive influence on fuel centerline temperature and fuel deformation caused by oxygen and plutonium profiles.[7,8] Teague et al. used a finite element method of microstructural modeling to model the thermal conductivity of a fixed high-burnup mixed oxide fuel.[9] Yun et al. studied the impact of high porosity on the thermal transport in the UO_2 fuel.[10] The fuel porosity was not considered in thermal conductivity model but in the fuel geometry by adding a certain number of spheres into the fuel. In addition to chemistry, high temperatures also affect fission gas release and swelling and finally cause the fuel porosity to increase. During irradiation the fast reactor fuel evolves dramatically due to fission gas release and swelling, creep of the fuel and cladding,

RONG LIU and WEI ZHOU, Ph.D. Students, and WENZHONG ZHOU, Assistant Professor, are with the Department of Mechanical and Biomedical Engineering, City University of Hong Kong, Hong Kong, China. Contact e-mail: wenzzhou@cityu.edu.hk

irradiation-induced effects, thermal diffusion of the fuel constituents, and fuel restructuring.

Hence, a reasonable approach to modeling a fast reactor fuel pellet should include thermal, mechanical, chemical, and fission gas behavior models in a coupled form, together with a complete material property data set.[2] Here the mixed oxide fast reactor fuel was further studied with burnup-dependent models, and more physical models were fully coupled together including thermal transport, deformation, fission gas release and swelling, grain growth, oxygen diffusion, and plutonium redistribution in a reactor fuel pellet.

II. MULTIPHYSICS MODELS

A. *Pellet Heat Conduction Model*

In modeling and simulation, a MOX fuel pellet of FBR was considered with a radius (α_{pel}) of 3.132 mm and a height of 1.5 mm (see Figure 1), which is a typical geometry of EBR-II. With this geometry, the thermal transport, oxygen diffusion, plutonium redistribution, and fission gas release problem were solved corresponding to a heat generation rate, Q, which is set to be proportional to plutonium concentration.[2] The heat transport equation is given by

$$\rho C_p \frac{\partial T}{\partial t} = \nabla \cdot (k \cdot \nabla T) + Q, \qquad [1]$$

where ρ, C_p, and k are the density, specific heat at constant pressure, and thermal conductivity, respectively. The heat flux q within the $(U_{1-y}, Pu_y)O_{2-x}$ fuel domain Ω can be written as[11]

$$q = -k\nabla T - Q^* D_O \nabla c_O, \qquad [2]$$

where k, D_O, and Q^* denote thermal conductivity, oxygen diffusion coefficient, and heat of transport of oxygen, respectively, and ∇c_O is the concentration gradient. For the configuration studied, both the concentration gradient and D_O are small, as is the actual transfer of mass due to oxygen and plutonium diffusion. The last term is therefore much smaller than $k\nabla T$ and thus it is neglected in this study, as in Reference 12.
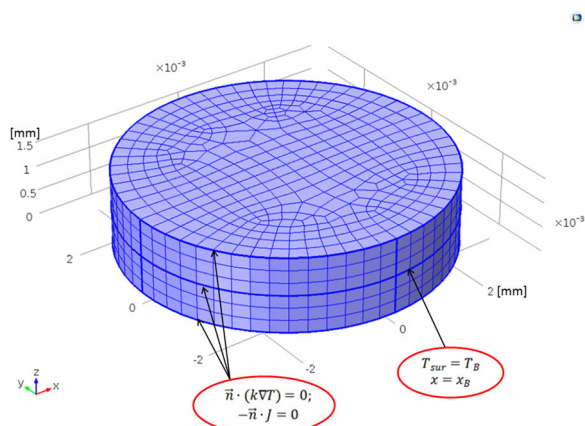

Fig. 1—Fuel geometry and modeling boundary conditions.

B. *Oxygen Diffusion Model*

As a radial redistribution of oxygen occurs due to the very large temperature gradient in the fuel, the OXIRED model is adopted to describe the radial redistribution of oxygen.[13] The deviation from the stoichiometry is designated as x:

$$x = \left| \frac{O}{U + Pu} - 2 \right|, \qquad [3]$$

where $\frac{O}{U+Pu}$ denotes the oxygen-to-metal ratio. Fast reactor fuels are purposely fabricated with a deficiency of oxygen (*i.e.*, hypo-stoichiometric), primarily to reduce the propensity for irradiated fuels to oxidize the cladding, which leads to "thinning" or "wastage." In the hypo-stoichiometric state, a pseudo-binary system is assumed, consisting of a dilute solution of oxygen vacancies in the oxygen sublattice. For hypo-stoichiometric fuel elements, the continuity equation is considered as follows:

$$N_O \frac{\partial C_O}{\partial t} = -\nabla J_O, \qquad [4]$$

where C_O denotes the atomic fraction of vacancies, J_O is the flux of oxygen vacancies, and N_O is the total number of oxygen atoms per unit volume. Then the thermal diffusion of oxygen vacancies in the hypo-stoichiometric mixed oxides can be described using flux equation derived from the thermodynamics of irreversible processes[14]; the flux of oxygen vacancies, J_O is given by

$$J_O = -N_O D_O \left[\nabla c_O + \frac{c_O(1 - c_O)}{F} \frac{Q_O^*}{RT^2} \nabla T \right], \qquad [5]$$

where D_O is the chemical diffusion coefficient, Q_O^* is the heat of transport, F is the thermodynamic factor, and R is the ideal gas constant. In Eq. [5], the gradient of non-stoichiometry is associated with the conventional Fickian diffusion contribution, whereas the term involving a gradient in temperature represents the thermal segregation or the Soret effect.[15] In the dilute limit, $x \to 0$, the thermodynamic factor has the limit $F \to 1$. For hypo-stoichiometric oxides, the atomic fraction of vacancies, c_O, is related to the deviation from stoichiometry, x, as

$$c_O = \frac{1}{2}x. \qquad [6]$$

C. *Plutonium Migration*

Plutonium redistribution has been modeled using the thermo-transport theory given in References 5 and 6. The diffusion current has concentration gradient and thermal diffusion terms. It is given as follows:

$$J_{Pu} = -D_{U-Pu} \left(\nabla y + y(1 - y) \frac{Q_{U-Pu}}{RT^2} \nabla T \right), \qquad [7]$$

where y and $(1 - y)$ are the molar fraction of plutonium and uranium oxides, respectively. Q_{U-Pu} is the effective molar heat of transport, and D_{U-Pu} is the

chemical interdiffusion coefficient. The continuity equation of plutonium redistribution is given as follows:

$$\frac{\partial y}{\partial t} = -\nabla J_{Pu}. \qquad [8]$$

D. Fuel Burnup Model

In order to accurately predict the fuel evolution, it is necessary to calculate the burnup of the fuel as a function of time and power history. The fuel burnup is calculated based on an ODE equation given by[16]

$$\frac{dBu}{dt} = \frac{P_{lin}((1-y)M_U + yM_{Pu} + (2-x)M_O)}{\pi a_{pel}^2 \rho_0((1-y)M_U + yM_{Pu})}, \qquad [9]$$

where Bu is the burnup (MW*h/kg), P_{lin} is the instantaneous linear power (W/m), a_{pel} is the fuel pellet initial radius (m), and ρ_0 is the density of unirradiated fuel. M_U is the atomic weight of natural uranium, M_{Pu} is the atomic weight of natural plutonium, and M_O is the atomic weight of oxygen.

E. Fuel Deformation

During reactor operation, nuclear fuel experiences structural changes and large temperature gradients, while new solid and gaseous species are introduced within the material due to fission. It is therefore expected that significant structural deformation will occur within the fuel. The fuel element deformation behavior is described using Cauchy's equation:

$$-\nabla \cdot \sigma = F_v, \qquad [10]$$

where σ is the Cauchy stress tensor and F_v is the body force per unit volume, which depends on applied forces, thermal expansion, material creep, fuel densification, and fission gas swelling. The stress is calculated with a liner elastic constitutive model:

$$\sigma = [C][\varepsilon], \qquad [11]$$

where C is the material matrix and ε is the elastic strain vector. The elastic strain is calculated as the total strain, defined as $1/2[\nabla \cdot u + \nabla \cdot u^T]$, (u is the displacement vector) minus any sources of inelastic strain.

Thermal expansion of the oxide fuel below the melting point is given in Reference 17 in the following form:

$$\varepsilon_{th} = \frac{\Delta L}{L_0} = K_1 T - K_2 + K_3 \exp\left(-\frac{E_D}{RT}\right), \qquad [12]$$

and K_1, K_2, K_3, and E_D are given in Table I for UO$_2$ and PuO$_2$. Given the concentration, $\frac{\Delta L}{L_0}$ values for UO$_2$ and PuO$_2$ are interpolated, and the densification strain is given as follows[18]:

$$\varepsilon_{dens} = \frac{1}{3}\frac{\Delta V_{dens}}{V} = \frac{1}{3}\left(\frac{1-P_0}{1-P_0(1-F_{dens})} - 1\right). \qquad [13]$$

The solid and gaseous fission products induced strain is calculated as[18]

Table I. Constants for the Fuel Thermal Expansion

Constant	UO$_2$	PuO$_2$	Units
K_1	1.0e−5	9.0e−6	K^{-1}
K_2	3.0e−3	2.7e−3	—
K_3	4.0e−2	7.0e−2	—
E_D	6.9e−20	7.0e−20	J

$$\varepsilon_{sfp} = \frac{1}{3}\frac{\Delta V_{sfp}}{V}, \qquad [14]$$

$$\varepsilon_{gfp} = \frac{1}{3}\frac{\Delta V_{gfp}}{V}, \qquad [15]$$

where $\frac{\Delta V_{sfp}}{V}$ and $\frac{\Delta V_{gfp}}{V}$ represent the swelling due to solid and gaseous fission products, respectively. The detailed models are given in Section III.

F. Fission Gas Release

The Booth diffusion model[19] is used to predict fission gas diffusion in this work due to its close agreement with the experimental results. The gas concentration c_g (atom/m^3) is determined by

$$\frac{\partial c_g}{\partial t} = D_g \frac{1}{r}\frac{\partial^2(rc_g)}{\partial r^2} + B, \qquad [16]$$

where D_g (m^2/s) is the diffusion coefficient of fission product gases. The source term B (atom/m^3/s) is the gas production rate from nuclear fission $B = \dot{F}z$, where $z = 0.25$ atom/fission is the yield of fission gas atoms. F (fissions/m^3/s) is the fission rate density based on a single fission event and contributes approximately 200 MeV of heat to the heat generation rate, such that

$$\dot{F} = \left[200\frac{MeV}{fission} \times \frac{10^6}{1\,MeV} \times \frac{1.6 \times 10^{-19}\,J}{eV}\right]^{-1}\left[Q\frac{J}{m^3 s}\right]$$
$$= (3.125 \times 10^{10})Q, \qquad [17]$$

where Q (W/m^3) is the heat generation rate given in 2.1. A two-dimensional rectangular domain is used in which one direction represents the radial coordinate of the grain within the fuel pellet and the other direction represents the radial coordinate within the spherical grain. Equation [16] was transformed to a non-dimensional form by substitution of $\eta = \frac{r}{g_r}$ to obtain

$$\eta^2 g_r^2 \frac{\partial c_g}{\partial t} = \frac{\partial c_g}{\partial \eta}\left(-D_g \eta^2 \frac{\partial c_g}{\partial \eta}\right) + \eta^2 g_r^2 B. \qquad [18]$$

Then the release rate to the grain boundary, R_{gb}, is

$$R_{gb} = \frac{3}{g_r^2} D_g \frac{\partial c_g}{\partial y}\bigg|_{y=1}, \qquad [19]$$

where g_r is the local fuel grain radius. It is assumed that fission gas atoms that diffuse to the grain boundary $(r = g_r)$ are immediately released to the

inter-granular porosity: $c_g(r = g_r) = 0$. The grain size is the radius of an equivalent sphere. During fuel irradiation, high temperature causes the grains of crystal lattice to grow, and Reference 20 suggests the following mixed oxide fuel grain growth correlation:

$$g_d^3 - g_0^3 = 1.11 \times 10^{12} \exp\left(-\frac{445870}{RT}\right)t \qquad [20]$$

where g_d is the grain diameter $2g_r$ (μm), g_0 is the initial grain size, and t is the time in minute.

Furthermore, the maximum allowed grain size is suggested by Reference 11 as follows:

$$g_{max} = 2200 \exp\left(-\frac{63000}{RT}\right). \qquad [21]$$

The Booth equation was solved analytically by Kidson to give the fractional release during k cycles of operation as[21]

$$F^k(t) = 1 - \sum_{n=1}^{\infty}\left(\frac{6}{n^4\pi^4}\right)\frac{\sum_{s=1}^{k}\left(\frac{B_s a_s^2}{D_s}\right)\left(1 - \exp\left(-\frac{n^2\pi^2 D_s t_s}{a_s^2}\right)\right)\exp\left(-\left(\sum_{r=1}^{k}\left(-\frac{n^2\pi^2 D_r t_r}{a_r^2}\right) - \sum_{r=1}^{s}\left(-\frac{n^2\pi^2 D_r t_r}{a_r^2}\right)\right)\right)}{\sum_{s=1}^{k} B_s t_s}, \qquad [22]$$

where s is the cycle number and r is "dummy" subscript used for summation. As fission gas atoms are released to the grain boundaries, with the increased burnup, gas atoms saturate the grain boundaries, causing the bubbles to interlink and thus creating a diffusion path to the free volume within the fuel free element. The saturated surface concentration is described by White et $al.$ as a "smear density" N_{sat} (atom/m^2) given by[22]

$$N_{sat} = \frac{4r_f f(\theta)f_B}{3k_B T \sin^2\theta}\left(P_{ext} + \frac{2\gamma}{r_f}\right). \qquad [23]$$

The commonly used value of N_{sat} from Reference 16 was adopted.

G. Material Properties

Material properties of the fuel $U_{1-y}Pu_yO_{2-x}$ were obtained from the literatures and are summarized in Table II, and the constants for the specific heat capacity of UO_2 and PuO_2 fuels are shown in Table III. The as-fabricated mixed oxide fuel thermal conductivity (k_0) is given as the sum of phonon and electron conduction. In addition, the correction factors are included to describe the effect of dissolved solid fission products (F_1), precipitated solid fission products (F_2), radiation damage (F_3), and porosity (F_4), namely

$$k = F_1 F_2 F_3 F_4 k_0. \qquad [24]$$

All these factors are summarized in Table II. The temperature dependence of thermal conductivity is illustrated in Figure 2. In Figure 2(a), an initial porosity of

0.028 is fixed, and then the thermal conductivities of three kinds of O/M ratios are compared. We can see that the O/M ratio has great influence on the fuel thermal conductivity, with a maximum difference of 2 W/(m K) between O/M = 1.9 and O/M = 1.999 at 300 K (23 °C). Then in Figure 2(b) the thermal conductivities with respect to different burnup (pct) levels are plotted, together with the thermal conductivity of different O/M ratios from MATPRO[17] for comparison. It is found that the fuel thermal conductivity decreases dramatically with the increase of the fuel burnup. The correlation developed by Carbajo et $al.$[23] is used for the $U_{1-y}Pu_yO_{2-x}$ fuel density, and the room-temperature density is given by

$$\rho_{[273 K]} = 10,970 + 490y(kg/m^3). \qquad [25]$$

For different temperature ranges, the fuel density used is presented in Table II, which is from Reference 24. The lattice specific heat capacity of solids at constant volume can be characterized theoretically quite well using the Debye model for specific heat. In the case of mixed oxide fuel, the specific heat capacity is based on Debye model with an extra contribution from defect energy, such as Frenkel defects and Schottky defects. The exact formulation is from Reference 17, which is listed in Table II, and the corresponding constants are summarized in Table III. Then the specific heat capacity is plotted with respect to temperature under different plutonium contents and O/M ratios, as shown in Figure 3. We can see that there is no substantial change under 2000 K (1727 °C) for both two different situations, and the plutonium content changes it slightly more than O/M ratio when the temperature is above 2000 K (1727 °C). The experimental heat capacity of $U_{0.8}Pu_{0.2}O_2$[25] is also shown in Figure 3(b) for comparison, and good agreement is observed between the modeling and experimental results. The evolved fuel porosity, accounting for fuel densification, and gaseous and solid fission product swelling, is given by

$$P = P_0\left(1 - F_{dens} - \frac{\Delta V_{sfp}}{V}\right) + \frac{\Delta V_{gfp}}{V}, \qquad [26]$$

where $P_0 = 0.028$ is the initial porosity of the fuel, F_{dens} is the fraction of the fuel porosity that is removed by densification, given as[26]

$$F_{dens} = 0.6 - \exp\left(-0.506 - 8.67 \times 10^{-10}T^3 \times \left(1 - \exp\left(2.867 \times 10^{-2}\beta\right)\right)\right), \qquad [27]$$

and $\frac{\Delta V_{sfp}}{V}$ is the swelling due to solid fission products, commonly represented as 0.32 pct per atom percent burnup[11]:

$$\frac{\Delta V_{\text{sfp}}}{V} = 0.0032\,\frac{\text{Bu}}{225}. \qquad [28]$$

The swelling due to gaseous fission products is predicted from MATPRO library for material properties of nuclear fuel[7]:

The model assumes that swelling stops once saturation occurs.

$$\frac{\mathrm{d}\left(\Delta V_{\text{gfp}}/V\right)}{\mathrm{d}t} = \begin{cases} 9.42 \times 10^{-36}(2800 - T)^{11.73}\exp(-0.0162(2800 - T))\exp\left(-8 \times 10^{-7}\text{Bu}\rho\right) \times \rho\frac{\mathrm{d}\text{Bu}}{\mathrm{d}t}, & \int_0^t F(t)B\mathrm{d}t \leq N_{\text{sat}}\frac{3}{a} \\ 0, & \int_0^t F(t)B\mathrm{d}t \geq N_{\text{sat}}\frac{3}{a} \end{cases}. \qquad [29]$$

Table II. Summary of Mixed Oxide $(U_{1-y}, Pu_y)O_{2-x}$ Fuel Properties

Property (Material)	Functional Form of the Property	Units	Source
Fuel density $\rho\ (U_{1-y}Pu_yO_{2-x})$	$(10970 + 490y)(a + bT + cT^2 + dT^3)^{-3}$, with (1) for $T \leq 923\,\text{K}(650\,^\circ\text{C})$: $a = 0.99734$, $b = 9.802 \times 10^{-6}$, $c = -2.705 \times 10^{-10}$, $d = 4.391 \times 10^{-13}$ (2) for $T > 923\,\text{K}(650\,^\circ\text{C})$: $a = 0.99672$, $b = 1.179 \times 10^{-5}$, $c = -2.429 \times 10^{-9}$, $d = 1.219 \times 10^{-12}$	kg/m³	[23, 24]
Heat capacity $C_p(U_{1-y}Pu_yO_{2-x})$	$C_p = yC_p^f(\text{PuO}_2) + (1 - y)C_p^f(\text{UO}_2)$ $C_p^f = \frac{K_1\theta^2 \exp\left(\frac{\theta}{T}\right)}{T^2\left[\exp\left(\frac{\theta}{T}\right)-1\right]^2} + K_2T + \frac{(2-x)K_3E_D}{2RT^2}\exp\left(-\frac{E_D}{RT}\right)$	J/(kg K)	[17]
Thermal conductivity $k(U_{1-y}Pu_yO_{2-x})$	$k = F_1F_2F_3F_4k_0$ $k_0 = \frac{1}{0.06059+0.2754\sqrt{\mid x \mid}+2.011\times10^{-4}T} + \frac{4.175\times10^9}{T^2}\exp\left(-\frac{16361}{T}\right)$ $F_1 = \left(\frac{1.09}{\text{Bu}^{3.265}} + \frac{0.0643}{\sqrt{\text{Bu}}}\sqrt{T}\right)\arctan\left(\frac{1}{\frac{1.09}{\text{Bu}^{3.265}} + \frac{0.0643}{\sqrt{\text{Bu}}}\sqrt{T}}\right)$ $F_2 = 1 + \frac{0.019\text{Bu}}{(3-0.019\text{Bu})}\frac{1}{1+\exp\left(-\frac{T-1200}{100}\right)}$ $F_3 = 1 - \frac{0.2}{1+\exp\left(\frac{T-900}{80}\right)}$ $F_4 = \frac{1-P}{1+\sigma P}$, $\sigma = 3$ $P = P_0\left(1 - F_{\text{dens}} - \frac{\Delta V_{\text{sfp}}}{V}\right) + \frac{\Delta V_{\text{gfp}}}{V}$	W/(m k)	[2,9]
Thermal expansion $\alpha(U_{1-y}Pu_yO_{2-x})$	$(a + bT + cT^2 + dT^3)$, with (1) for $T \leq 923\,\text{K}(650\,^\circ\text{C})$: $a = 9.828 \times 10^{-6}$, $b = -6.390 \times 10^{-10}$, $c = 1.33 \times 10^{-12}$, $d = -1.757 \times 10^{-17}$ (2) for $T > 923\,\text{K}(650\,^\circ\text{C})$: $a = 1.183 \times 10^{-5}$, $b = -5.013 \times 10^{-9}$, $c = 3.756 \times 10^{-12}$, $d = -6.125 \times 10^{-17}$	K⁻¹	[23]
Poisson ratio $v(U_{1-y}Pu_yO_{2-x})$	$(1 - y) * v(\text{UO}_2) + y * v(\text{PuO}_2)$ $v(\text{UO}_2) = 0.316 + (0.5 - 0.316) * (T - 300)/2800$ $v(\text{PuO}_2) = 0.276 + (0.5 - 0.276) * (T - 300)/2800$	—	[11, 17]
$Q_O^*\ (U_{1-y}Pu_yO_{2-x})$	$-8.12 \times 10^{-4}\exp(4.85V_{\text{Pu}})$, $V_{\text{Pu}} = 4 - 2x/y$	J/mol	[4]
D_O	$1.39 \times 10^{-6} \times \exp(-9128/T)$	m²/s	[4]
$Q_{\text{U-Pu}}$	$-35,000$	cal/mol	[5]
$D_{\text{U-Pu}}$	$3.4 \times 10^{-5}\exp(-55351/T)$	m²/s	[5]

Table III. Constants for the Specific Heat Capacity of UO₂ and PuO₂

Table III.   Constants for the Specific Heat Capacity of UO_2 and PuO_2

Constant	UO_2	PuO_2	Units
K_1	296.7	347.4	J/kg K
K_2	2.43×10^{-2}	3.95×10^{-4}	J/kg K^2
K_3	8.745×10^7	3.86×10^7	J/kg
θ	535.285	571.0	K
E_D	1.577×10^5	1.967×10^5	J/mol
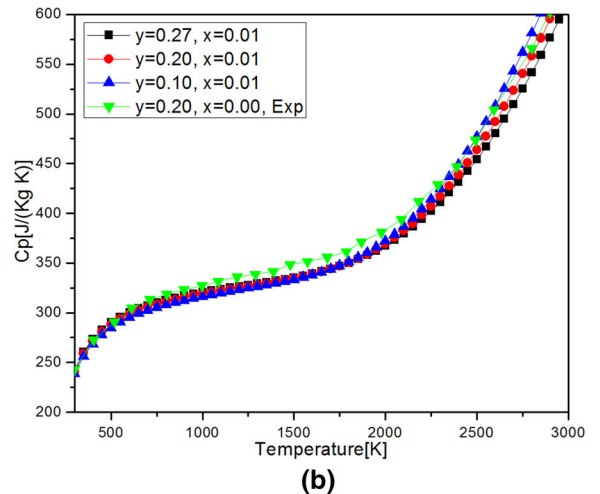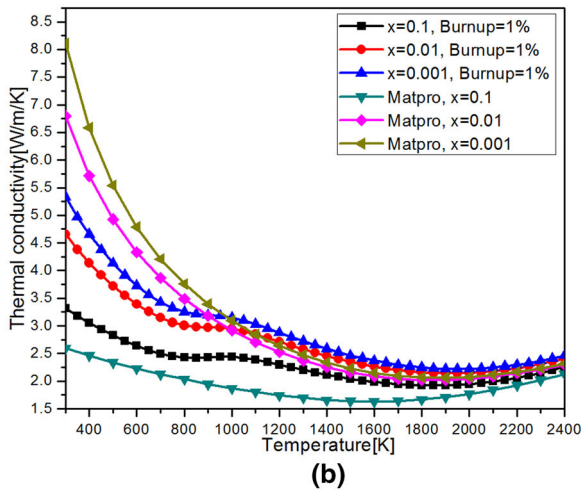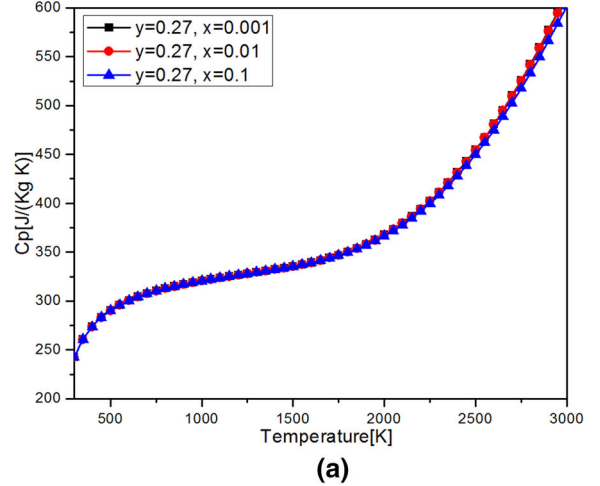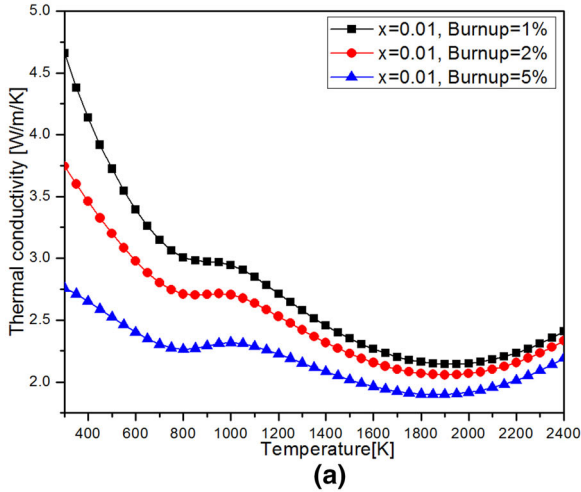
Fig. 2—(a) Fuel thermal conductivity with a deviation from stoichiometry of oxygen of 0.1 at three different burnups of 1, 2, and 5 pct; (b) fuel thermal conductivity with three deviations from stoichiometry of oxygen of 0.1, 0.01, and 0.001 at a burnup of 1 pct, together with the thermal conductivity from MATPRO model for three deviations from stoichiometry of oxygen of 0.1, 0.01, and 0.001.

Fig. 3—(a) Fuel heat capacity with a plutonium content of 0.27 and different deviations from stoichiometry of oxygen (x) of 0.1, 0.01, and 0.001; (b) fuel heat capacity with a deviation from stoichiometry of oxygen (x) of 0.01 and three different plutonium contents of 0.10, 0.20, and 0.27, together with the experimental heat capacity of $(U_{0.8}Pu_{0.2})O_2$ for comparison.

III.   RESULTS AND DISCUSSION

The simulations were performed on the framework of COMSOL Multiphysics, and the solutions of the fuel performance problem were obtained by solving fully coupled multiphysics models. The conduction component of the Heat Transfer Module in COMSOL Multiphysics was used to solve heat transport in the fuel. The thermal deformation was calculated using the linear elastic deformation component of the Structural

Mechanics Module in transient regime. The rest, such as oxygen diffusion, plutonium redistribution, grain growth, fission gas swelling and release models, are implemented with self-defined PDEs into COMSOL Multiphysics. For the burnup calculation, a Domain ODEs and DAEs module was used to calculate the local and average burnups. The numerical solutions of the coupled multiphysics problem were obtained using the default linear solver Multi-frontal Massively Parallel
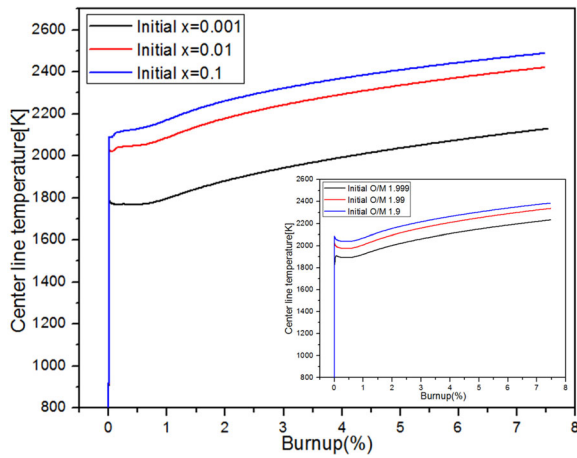
Fig. 4—Fuel centerline temperature with the evolution of burnup and an initial Pu content (y) of 0.27; inset shows the fuel centerline temperature evolution without considering fission gas release-induced porosity.

Fig. 5—Fuel porosity against the evolution of burnup with three different initial deviations from stoichiometry of oxygen (x).

sparse direct Solver (MUMPS) in COMSOL Multiphysics. The finite element mesh uses swept meshes, and we verified that the numerical results converged with respect to mesh-size distribution. Only transient simulations were considered corresponding to burnup-dependent models in the simulations.

As stated in Section II, a heat source Q was considered which is calculated as $Q = \frac{P_{lin}}{\pi a_{pel}^2} \times \frac{y}{y_{ave}}$, where y is the molar fraction of plutonium oxide and y_{ave} is the fuel pin average molar fraction of plutonium oxide. A linear power of 35 kW/m was applied in all our simulations. An "flc1hs" smoothed Heaviside function was used to avoid unnecessary numerical instability in the model. For the boundary conditions, as illustrated in Figure 1, we consider three kinds of initial plutonium content (y), namely 0.27, 0.2, and 0.1. The temperature at the outer surface of the fuel is fixed to the initial temperature, T_{sur} = 800 K (527 °C); for the top and bottom of the fuel pellet, it is set such that there is no heat flux. Dirichlet boundary condition was applied to the fuel surface with three types of deviation from stoichiometry of oxygen (0.001, 0.01, 0.1). All the models are coupled and simulated up to a burnup of about 7.5 pct.

First, the $(U_{1-y}Pu_y)O_{2-x}$ fuel performance with y = 0.27 was studied with the conditions of three kinds of deviation from stoichiometry of oxygen (0.001, 0.01, 0.1). As shown in Figure 4, the temperature is found to be very sensitive to a small change in deviation from stoichiometry of oxygen. About 300 K (27 °C) temperature difference occurs between the cases of 0.001 and 0.1 at the beginning of fuel burnup, which is similar to the simulation result of Mihhla et al.[7] even though different kinds of thermal conductivity models were used. A burnup-dependent degraded thermal conductivity model was adopted as shown in Figure 2. As we can see from Figure 4, the fuel centerline temperature first increased slightly due to the increase of the fuel porosity and then increased dramatically with the increase of the fuel burnup, except for the case with an
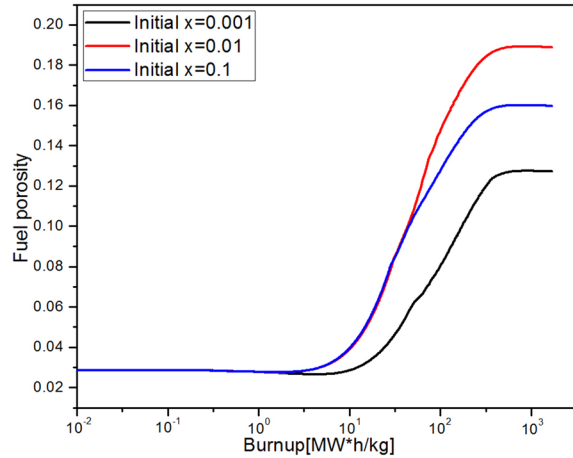
initial deviation from stoichiometry of oxygen of 0.001 due to the smallest porosity change compared with the other two cases. The inset of Figure 4 shows the fuel centerline temperature evolution without considering the fission gas-induced porosity. There is no clear temperature increase at the beginning of the fuel burnup compared to the case considering fission gas-induced porosity. The fuel centerline temperature of the case considering the fission gas-induced porosity is found to increase to about 50 K (50 °C) at the beginning of fuel burnup and be about 100 K (100 °C) higher than the case without considering the fission gas-induced porosity at the burnup of 7.5 pct owing to the fuel thermal conductivity degradation caused by fission gas-induced porosity as shown in Eq. [24] and Table II.

The porosity evolution was then plotted against the fuel burnup, as depicted in Figure 5. There is a tiny decrease at the very beginning of the fuel burnup, which is caused by fuel densification process. Then the porosity increases in a very short period until a saturated maximum value is reached, for example, at about 0.19 for the case of initial deviation from stoichiometry of oxygen of 0.01, as the fission gas releases to the free fuel volume after the fuel grain boundary got saturated, corresponding to the period when the temperature increases. The saturated porosity is determined not only by temperature, but a combination of O/M ratio, plutonium content, temperature, and fission gas release in the fuel grain boundary. So, in Figure 5, the saturated porosity is no more reversely proportional to the initial deviation from stoichiometry of oxygen, i.e., the highest saturated porosity of about 0.19 obtained for the case of initial deviation from stoichiometry of oxygen of 0.01, the lowest saturated porosity of about 0.127 obtained for the case of initial deviation from stoichiometry of oxygen of 0.001, and the saturated porosity of about 0.16 obtained for the case of initial deviation from stoichiometry of oxygen of 0.1 in between the above two cases.

The fuel grain size evolution is plotted against the burnup in Figure 6 for the fuel centerline. The fuel grain size is found to be proportional to the temperature and increases with respect to the fuel temperature increase as
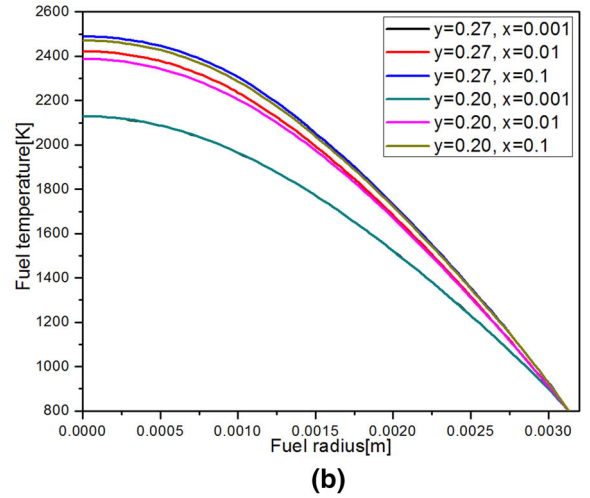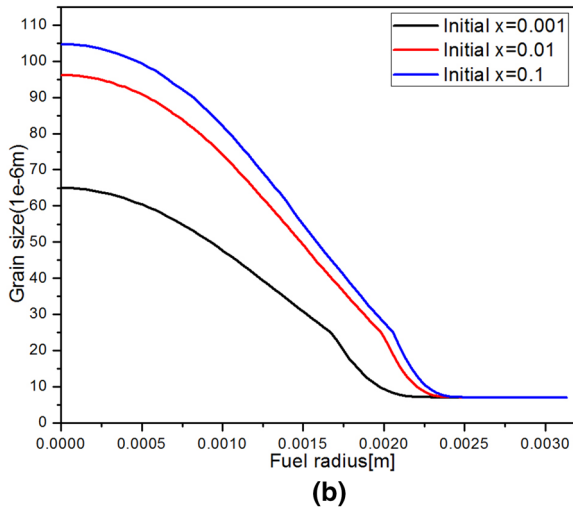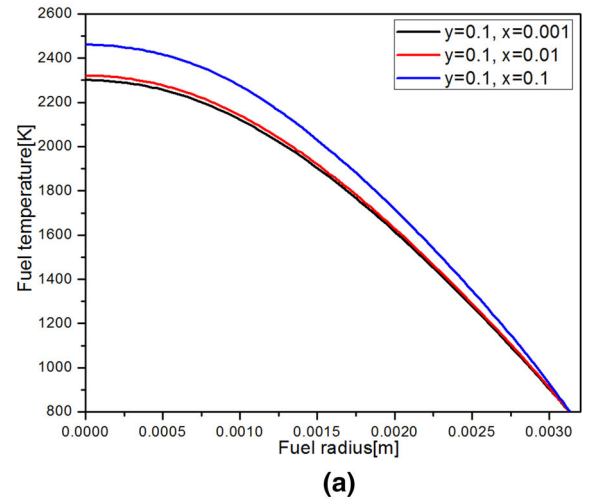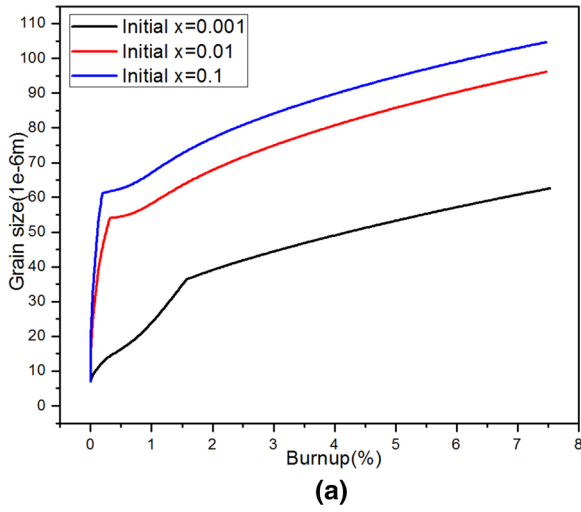
(a)

(b)

Fig. 6—(a) Fuel grain size against the evolution of burnup; (b) fuel radial grain size distribution at the middle height of the fuel, both with different initial deviations from stoichiometry of oxygen (x).

(a)

(b)

Fig. 8—(a) Fuel radial temperature distribution with three initial deviations from stoichiometry of oxygen (x) and an initial Pu content of 0.1; (b) fuel radial temperature distribution with two different initial Pu contents (y) and three initial deviations from stoichiometry of oxygen (x), both at the burnup of 7.5 pct.
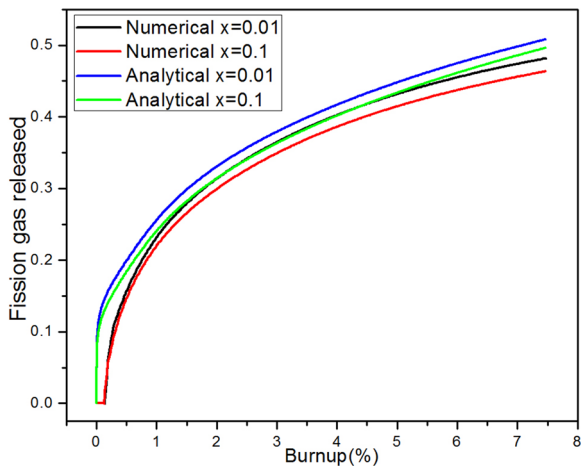

Fig. 7—Analytical and numerical results of fission gas release with two different initial deviations from stoichiometry of oxygen (x).

shown in Figure 6(a). The radial fuel grain size is found to decrease from the fuel center to the outer surface as shown in Figure 6(b), which is reasonable compared with Reference 20, in which the grain growth occurs where temperature is over about 1300 K (1027 °C). The deviation from stoichiometry of oxygen has significant effect on the grain size evolution as shown in Figure 6. At the burnup of 7.5 pct, the fuel grain size is about 65 μm for the case of initial deviation from stoichiometry of oxygen of 0.001; however, the fuel grain sizes can reach about 96 and 105 μm for the cases of initial deviations from stoichiometry of oxygen of 0.01 and 0.1, respectively. This can be explained that when the deviation from stoichiometry of oxygen increases, thermal conductivity decreases according Eq. [24] and Table II, then the fuel temperature increases, resulting in the fuel grain size increase finally according to Eq. [20].

Further assessment of the fission gas release model was performed. As shown in Figure 7, both analytical and numerical results were plotted. The fission gas release
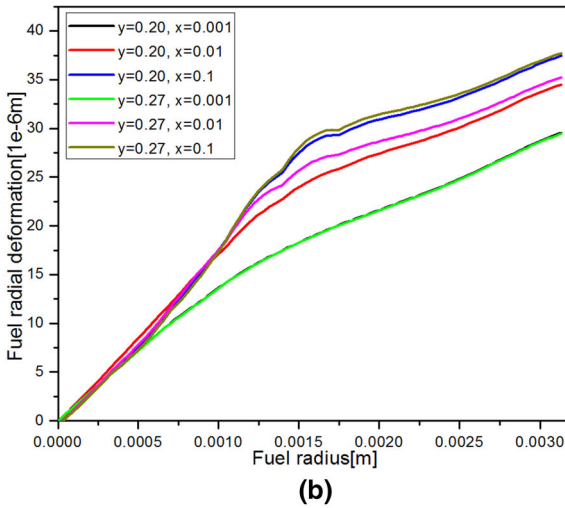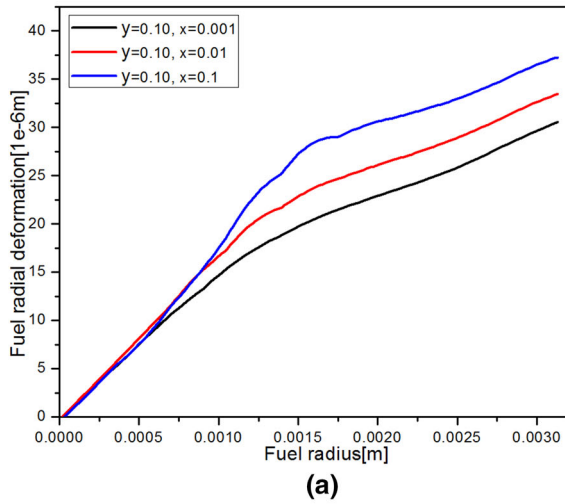
(a)

(b)

Fig. 9—(*a*) Fuel radial deformation with three initial deviations from stoichiometry of oxygen (*x*) and an initial Pu content of 0.1; (*b*) fuel radial deformation with two different initial Pu contents (*y*) and three initial deviations from stoichiometry of oxygen (*x*), both at the burnup of 7.5 pct.

Fig. 10—Fuel radial Pu content with three different initial deviations from stoichiometry of oxygen (*x*) at the burnup of 7.5 pct.

relatively small or large. At the burnup of 7.5 pc, the fuel centerline temperatures are about 2488 K, 2420 K, and 2128 K (2215 °C, 2147 °C, and 1855 °C) for different initial deviations from stoichiometry of oxygen of 0.1, 0.01, and 0.001, respectively, as shown in Figure 8(a); and the fuel deformations at the centerline are 37.73, 35.27, and 29.50 *μ*m for different initial deviations from stoichiometry of oxygen of 0.1, 0.01 and 0.001, respectively, as shown in Figure 9(a). However, the plutonium content affects slightly the fuel temperature distribution and deformation, as depicted in Figures 8(b) and 9(b).

Finally, plutonium content was plotted across fuel radius with a fuel burnup of 7.5 pct for different deviations from stoichiometry of oxygen, as shown in Figure 10. The plutonium redistribution is a slow process and tends to diffuse to the fuel center, which is found to be consistent with the work done by Di Marcello *et al.*[27] The plutonium content migration in the fuel is significantly affected by the deviation from stoichiometry of oxygen as shown in Figure 10. At the burnup of 7.5 pct, the plutonium content at the fuel centerline is about 0.308 for the case of initial deviation from stoichiometry of oxygen of 0.1; it is about 0.294 for the case of initial deviation from stoichiometry of oxygen of 0.01; and it is about 0.2712, only slightly higher than the initial Pu content of 0.27, for the case of initial deviation from stoichiometry of oxygen of 0.001. This can be explained that the deviation from stoichiometry of oxygen increases, thermal conductivity decreases according Eq. [24] and Table II, and then the fuel temperature increases, resulting in the increase of fuel plutonium migration to the center finally according to Eq. [7] and Table II.

IV. CONCLUSIONS

In summary, the $(U_{1-y}Pu_y)O_{2-x}$ mixed oxide fuel performance has been modeled in a fast reactor with fully coupled physics models based on the framework of COMSOL Multiphysics, and new burnup-dependent models were adopted. The modeling results showed a

increases logarithmically with the burnup increase, showing good agreement with the result from Adyin's work[2]: fission gases diffuse to the grain boundary, accumulate at the grain boundary, and then release to the free volume (that is why we find no fission gas release at the beginning of fuel burnup). The deviation from stoichiometry of oxygen is reversely proportional to the fission gas release. It is also found that the numerical method predicts lower results compared to the analytical method. However, the general trends are found to be consistent in both numerical and analytical methods.

The radial temperature distribution and deformation were compared among different kinds of initial plutonium contents and deviations from stoichiometry of oxygen at the end of calculated burnup, as depicted in Figures 8 and 9. The fuel temperature and deformation are found to be very sensitive to large deviation from stoichiometry of oxygen no matter plutonium content is
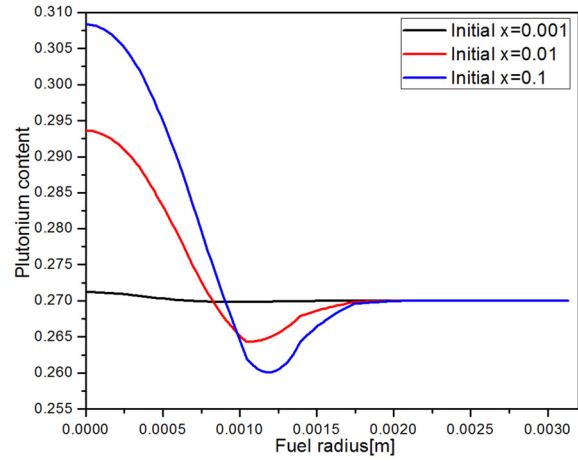
consistent fuel performance comparable with the previous results. Burnup degrades the thermal conductivity of the fuel and results in a significant increase in the fuel centerline temperature. It was also found that the fuel porosity increased dramatically at the beginning of the fuel burnup and then kept constant as the fission gas released to the fuel free volume. The porosity is found to cause about 50 K (50 °C) increase in fuel centerline temperature. The fission gas release model was simulated by numerical and analytical methods. Even though the numerical result is lower compared to the analytical result, the results of these two methods show good agreement with the previous work. Another important finding is that the deviation from stoichiometry of oxygen plays a significant role in fuel material properties and performance. The deviation from stoichiometry of oxygen affects greatly not only the fuel properties, for example, thermal conductivity, but also the fuel performance, for example, temperature distribution, porosity evolution, grain size growth, fission gas release, deformation, and plutonium redistribution. Special attention needs to be paid to the deviation from stoichiometry of oxygen in the fuel fabrication. Plutonium content also affects the fuel material properties and performance. However, it is not that significant compared to the deviation from stoichiometry of oxygen due to the similar material properties of UO_2 and PuO_2.

Overall, an effective approach was developed using self-defined multiphysics models based on the framework of COMSOL Multiphysics to manage the nonlinearities associated with fast reactor mixed oxide fuel performance analysis. Our modeling and simulation approach is of particular importance since it demonstrates that highly interrelated and nonlinear fuel performance models can be developed and implemented into a multiphysics platform, and thus more efforts can be put into physics model development and improvement. The modeling results can be used to identify the important phenomena and parameters, to direct and design experiments, and to assist in post analysis of expensive nuclear experiments for fast reactor nuclear fuel performance analysis.

REFERENCES

1. K. Maeda, S. Sasaki, M. Kato, and Y. Kihara: *J. Nucl. Mater.*, 2009, vol. 389 (1), pp. 78–84.
2. A. Karahan: Ph.D. Thesis, Massachusetts Institute of Technology, 2009.
3. M. Ishida, T. Ogata, and M. Kinoshita: *Nucl. Technol.*, 1993, vol. 104 (1), pp. 37–51.
4. K. Lassmann: *J. Nucl. Mater.*, 1987, vol. 150 (1), pp. 10–16.
5. C.F. Clement and M.W. Finnis: *J. Nucl. Mater.*, 1978, vol. 75 (1), pp. 193–200.
6. T. Ishii and T. Asaga: *J. Nucl. Mater.*, 2001, vol. 294 (1–2), pp. 13–17.
7. B. Mihaila, M. Stan, and J. Crapps: *J. Nucl. Mater.*, 2012, vol. 430 (1–3), pp. 221–28.
8. B. Mihaila, M. Stan, J. Crapps, and D. Yun: *J. Nucl. Mater.*, 2013, vol. 433 (1–3), pp. 132–42.
9. M. Teague, M. Tonks, S. Novascone, and S. Hayes: *J. Nucl. Mater.*, 2014, vol. 444 (1–3), pp. 161–69.
10. D. Yun and M. Stan: *J. Mater. Res.*, 2013, vol. 28 (17), pp. 2308–15.
11. D. Olander: Fundamental Aspects of Nuclear Reactor Fuel Elements, Technical Information Center, Energy Research and Development Administration, 1976.
12. J.C. Ramirez, M. Stan, and P. Cristea: *J. Nucl. Mater.*, 2006, vol. 359 (3), pp. 174–84.
13. C. Sari and G. Schumacher: *J. Nucl. Mater.*, 1976, vol. 61 (2), pp. 192–202.
14. S.R.D. Groot: *Thermodynamics of Irreversible Processes*, North Holland Publ. Co, Amsterdam, 1951.
15. C. Korte, J. Janek, and H. Timm: Solid State Ionics, 1997, vol. 101–103, Part 1(0), pp. 465–70.
16. D. Morgan: MASc Thesis, Royal Military College of Canada, 2007.
17. C.M. Allison, G.A. Berna, R. Chambers, E.W. Coryell, K.L. Davis, D.L. Hagrman, D.T. Hagrman, N.L. Hampton, J.K. Hohorst, R.E. Mason, M.L. McComas, K.A. McNeil, R.L. Miller, C.S. Olsen, G.A. Reymann, and L.J. Siefken: SCDAP/RELAP5/MOD3.1 Code Manual Volume IV: MATPRO-A Library of Materials Properties for Light-Water-Reactor Accident Analysis, NUREG/CR-6150, 1993.
18. K. Shaheen: Ph.D. Thesis, Royal Military College of Canada, 2011.
19. A.H. Booth: A Method of Calculating Fission Gas Diffusion from UO_2 Fuel and Its Application to the X-2-f Loop Test. AECL, 1957. 496.
20. C. Sari: *J. Nucl. Mater.*, 1986, vol. 137 (2), pp. 100–06.
21. G.V. Kidson: *J. Nucl. Mater.*, 1980, vol. 88 (2–3), pp. 299–308.
22. R.J. White and M.O. Tucker: *J. Nucl. Mater.*, 1983, vol. 118 (1), pp. 1–38.
23. J.J. Carbajo, G.L. Yoder, S.G. Popov, and V.K. Ivanov: *J. Nucl. Mater.*, 2001, vol. 299 (3), pp. 181–98.
24. J.K. Fink: *J. Nucl. Mater.*, 2000, vol. 279 (1), pp. 1–18.
25. R.L. Gibby, L. Leibowitz, J.F. Kerrisk, and D.G. Cliffton: *J. Nucl. Mater.*, 1974, vol. 50 (2), pp. 155–61.
26. I.J. Hastings and L.E. Evans: *J. Am. Ceram. Soc.*, 1979, vol. 62 (3–4), pp. 217–18.
27. V. Di Marcello, A. Schubert, J. van de Laar, and P. Van Uffelen: Revision of the transuranus PUREDI model, Technical report for the JRC-ITU Action No. 52201—Safety of Nuclear Fuels and Fuel cycles, European Commission, Joint Research Centre, Institute for Transuranium Elements, 2012.